ACS OMEGA

Open Access

http://pubs.acs.org/journal/acsodf

Article

Enhancement of Local Osseointegration and Implant Stability of Titanium Implant in Osteoporotic Rats by Biomimetic Multilayered Structures Containing Catalpol

Jiayi Yang,[‖] Wei Zhang,[‖] Binghao Lin, Shuming Mao, Guangyao Liu, Kai Tan, and Jiahao Tang*

Cite This: *ACS Omega* 2024, 9, 29544−29556

Read Online

ACCESS | Metrics & More | Article Recommendations

ABSTRACT: This study examined the surface modification of titanium (Ti) implants to enhance early-stage osseointegration, which reduced the failure rate of internal fixation in osteoporotic fractures that inherently decrease in bone mass and strength. We employed a layer-by-layer electroassembly technique to deposit catalpol-containing hyaluronic acid/chitosan multilayers onto the surface of Ti implants. To evaluate the in vitro osteoinductive effects of catalpol-coated Ti implants, the robust osteoblast differentiation capacity of the murine preosteoblast cell line, MC3T3-E1, was employed. Furthermore, the performance of these implants was evaluated in vivo through femoral intramedullary implantation in Sprague−Dawley rats. The engineered implant effectively regulated catalpol release, promoting increased bone formation during the initial stages of implantation. The in vitro findings demonstrated that catalpol-coated Ti surfaces boosted ALP activity, cell proliferation as measured by CCK-8, and osteogenic protein expression via WB analysis, surpassing the uncoated Ti group ($P < 0.05$). In vivo micro-computed tomography (CT) and histological analyses revealed that catalpol-coated Ti significantly facilitated the formation and remodeling of new bone in osteoporotic rats at 14 days post-implantation. This study outlines a comprehensive and straightforward methodology for the fabrication of biofunctional Ti implants to address osteoporosis.

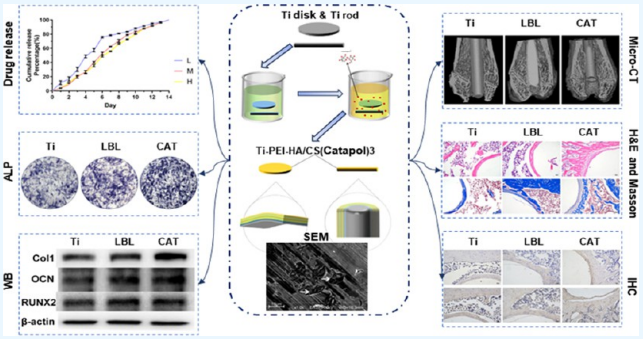

1. INTRODUCTION

Titanium (Ti) and its alloys stand out as exemplary biomaterials, possessing superior qualities such as exceptional bioinertness, biocompatibility, high fatigue and tensile strengths, low allergenicity, and lightweight.[1] These attributes render them extensively utilized in orthopedic and dental implants. However, the bioinert nature of Ti-based implants makes it challenging to establish a robust chemical bond with the surrounding bone, particularly during the early stages of implantation.[2] Moreover, the degradation of metallic implants like titanium within the biological environment can result in the liberation of metal ions, which have the potential to elicit both local and systemic responses, and may also provoke allergic reactions.[3,4] These limitations impact early osseointegration, leading to adverse outcomes such as aseptic loosening of prostheses[5] and failure of intramedullary nail fixation. Periprosthetic fractures, which are common postoperative complications in total knee arthroplasty (TKA), are also influenced by the material properties of Ti, with the femur being the most frequent fracture site, followed by the tibia and patella.[6,7] Hence, recent research has focused on the surface modification of titanium substrates to enhance functionalization in the development of titanium implants.

Currently, two primary strategies are employed for titanium implant functionalization. The first involves the incorporation of growth factors into the surface to create an active implant tissue surface that stimulates bone cell growth.[8] Research has shown that the sustained release of BMP-2 in composite coatings notably enhances the proliferation and differentiation of MC3T3-E1 cells on titanium surfaces.[9] The second strategy involves the use of anabolic drugs to create biological coatings that exert a long-term and effective role in osseointegration by controlling drug release.[10] Studies have demonstrated that the immobilization of icariin, a key active constituent of Herba Epimedii, improves osteogenesis in a multilayer with hyaluronic acid (HA) and chitosan (CS) on a phase-transited lysozyme-primed Ti surface and can enhance early osseointegration in a rat model through sustained release.[11] Consequently, we explored

Received: March 9, 2024
Revised: June 13, 2024
Accepted: June 21, 2024
Published: June 28, 2024

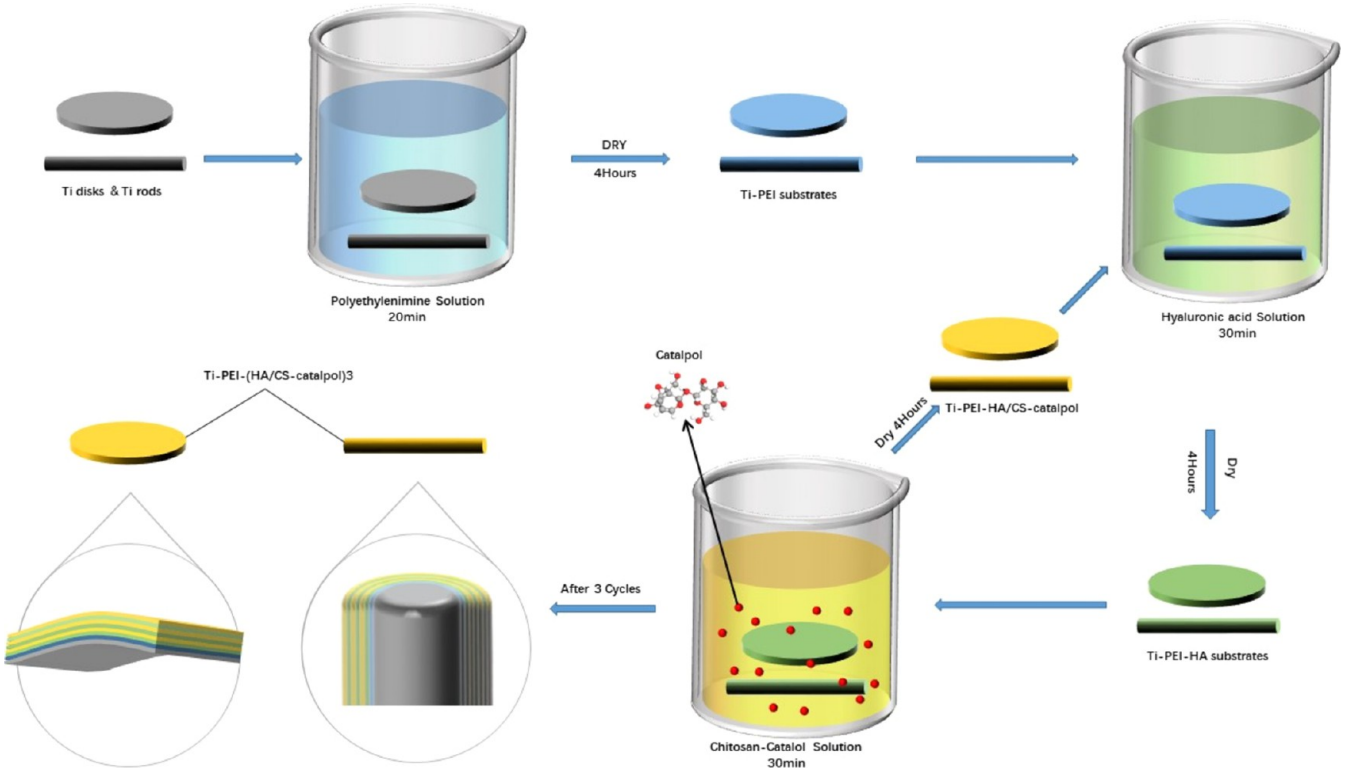

Figure 1. Illustrative representation of the sample preparation process: This entails the fabrication of HA/CS-CAT multilayer films on Ti disk or rod surfaces that have been primed with PEI.

the prospect of selecting suitable bioactive components from traditional Chinese medicine for loading onto titanium implants.

To facilitate the adhesion of coatings onto implant surfaces, the application of poly(ethylenimine) (PEI) is an effective strategy to achieve robust binding. Recognized as a cationic polymer, PEI boasts significant pH-buffering capabilities, often referred to metaphorically as a "proton sponge".[12] It is extensively utilized in the fields of gene therapy and drug delivery systems. The cytotoxic potential of PEI is subject to variation based on factors such as molecular weight and structural alterations; an increase in molecular weight correlates with heightened cytotoxicity.[13] Furthermore, the coadministration of HA with PEI has been shown to ameliorate the cytotoxic effects typically associated with PEI.[14]

Catalpol, the principal active component of Rehmanniae Radix, is a widely used herbal medicine in East Asia,[15] possesses diverse biological activities, including antioxidative,[16] anti-inflammatory,[17] and anti-ischemic effects.[18] Catalpol can also reduce blood glucose[19] and attenuate ischemic stroke.[20] Previous studies have confirmed the positive impact of catalpol on osteogenesis, enhancing bone healing in critical-sized calvarial defects in rats and mitigating bone loss in ovariectomized (OVX) rat models.[21] Additionally, catalpol has demonstrated protective effects against damage induced by 2,3,7,8-tetrachlorodibenzo-p-dioxin in MC3T3-E1 osteoblastic cells.[22] Although the exact osteogenic mechanism of catalpol remains unclear, numerous research findings suggest the crucial involvement of the Wnt/β-catenin pathway[23−25] and its role in bone mass regulation through Th1/Th2 adjustments, ultimately influencing bone loss related to estrogen deficiency.[26] Therefore, coating catalpol onto Ti substrate is a promising option.

In our study, catalpol was applied to a Ti substrate using layer-by-layer assembly.[27] Hyaluronic acid and chitosan were chosen to create multilayer films containing catalpol, with polyethylene serving as the base film to enhance adhesion between the titanium substrate and multilayers. Catalpol incorporation into the HA/CS layers occurs through electrostatic interactions, leading to catalpol encapsulation within the microinterspaces of the three-dimensional (3D) HA/CS network.[28] Notably, both HA and CS exhibited potent antibacterial properties, contributing to a reduced incidence of implant infection.[29,30]

In this study, we engineered Ti implants coated with a biological multilayer film containing catalpol and thoroughly analyzed the characteristics of the coating and encapsulation of catalpol within different cover layers in HA/CS films. Furthermore, we investigated the influence of the film architecture on the drug release mechanism. In vitro evaluations using the murine preosteoblast cell line MC3T3-E1, renowned for its osteoblast differentiation potential, evaluated the impact of multilayered HA/CS-coated Ti substrates with catalpol on osteoinductive properties. Additionally, the positive impact of local drug release during the early stages of implantation was demonstrated in Sprague−Dawley rats using a surgical femoral intramedullary implantation paradigm in vivo.

2. MATERIALS AND METHODS

Trypsin, fetal bovine serum (FBS), phosphate-buffered saline (PBS), penicillin-streptomycin, and α minimum essential medium (α-MEM) were obtained from Thermo Fisher Scientific (Waltham, MA).

2.1. Specimen Preparation. *2.1.1. Fabrication of the Titanium-PEI Substrate.* In this study, we utilized a Ti6Al4 V Titanium alloy from Baoji Titanium Industry Co. Ltd. Two sample forms were prepared: Ti rods (15 mm length, 1.5 mm diameter) and Ti disks (0.3 mm thickness, 14 mm diameter). After meticulous polishing, the samples were ultrasonically

https://doi.org/10.1021/acsomega.4c02322
ACS Omega 2024, 9, 29544−29556

cleaned with acetone, 70% ethanol, and sterile deionized water and dried at 60 °C for 1 h. To ensure a controlled foundation, the samples were immersed in a 5 mg/mL poly(ethylenimine) (PEI, 99%, 1800MW, Solarbio Life Sciences, Beijing, China) solution with a pH of 9.0 for 20 min. Ti-PEI substrates were air-dried for 4 h, creating a uniform surface for subsequent analyses of the material properties.

2.1.2. Preparation of Layer-by-Layer with Catalpol Coatings on the Ti-PEI Substrates. Figure 1 shows the preparation of multilayer HA/CS-catalpol films on titanium substrates. First, sodium hyaluronate (HA, Bloomage Biotechnology Co. Ltd. Jinan, Shandong, China) solution (1 mg/mL, pH 2.9) was prepared in ddH_2O, and the Ti-PEI substrate was immersed in the HA solution for 30 min, and then air-dried at room temperature for 4 h to obtain the Ti-PEI-HA substrate. Subsequently, 1 g of chitosan was dissolved in water containing 1% v/v glacial acetic acid using a magnetic stirrer, and the total volume of this solution was 1000 mL, thereby preparing a chitosan (CS, deacetylation degree of 80%, and viscosity of 200 mPa·s; Solarbio Life Sciences, Beijing, China) solution. Then, CS-catalpol solutions with concentrations of 0.5×10^{-3} mol/L (catalpol-low), 1×10^{-3} mol/L (catalpol-medium), and 2×10^{-3} mol/L (catalpol-high) were prepared by dissolving different amounts of catalpol (Solarbio Life Sciences. Beijing, China) in the CS solution by means of a magnetic stirrer. The Ti-PEI-HA substrates were then immersed in CS solutions without or with the indicated concentrations of catalpol for 30 min and air-dried for 4 h at room temperature. The Ti-PEI samples were repeatedly immersed in HA and CS solutions for 3 cycles to form a multilayered HA/CS-catalpol coating (Figure 1) and then stored at 4 °C under sterile conditions. The final Ti-PEI-(HA/CS)s substrates, Ti-PEI-HA/CS-(catalpol-low) substrates, Ti-PEI-HA/CS-(catalpol-medium) substrates, and Ti-PEI-HA/CS-(catalpol-high) substrates were referred to as LBL, CAT-L, CAT-M, and CAT-H, respectively.

2.2. Characterization of Titanium Substrate Surfaces. The surface morphologies and characteristics of Ti, Ti-PEI, Ti-PEI-HA, Ti-PEI-HA/CS, LBL, and CAT were analyzed using a scanning electron microscope (Hitachi S-4800 SEM) from Hitachi Limited, Tokyo, Japan. Transmittance scans were performed in the range of 500−4000 cm^{-1} using a Fourier transform infrared spectrometer (Thermo Nicolet NEXUS 470 FTIR) from Thermo Fisher Scientific to determine the molecular composition of the Ti substrates. Images of liquid droplets were captured with a volume of 2 μL using an OCA 25 system equipped with a digital camera from Data Physics Instruments GmbH. Subsequently, contact angle measurements were performed using SCA 20 module analysis software (Data Physics Instruments GmbH, Germany).

2.3. In Vitro Drug Release Profiles. An ultraviolet−visible dual-beam spectrophotometer was used to obtain optical density (OD) readings for catalpol at known concentrations (0.078, 0.01, 0.02, 0.039, 0.078, 0.156, 0.3125, 0.625, 1.2, 2.5, and 5 mg/mL) to construct a standard curve. Catalpol concentrations liberated from different HA/CS substrates were evaluated using a standard curve. CAT-L, CAT-M, or CAT-H substrates were submerged in PBS and subjected to drug release at 37 °C. At specific intervals (each day), the substrates were removed and the residual PBS solution was analyzed by UV−visible spectrophotometry. The substrates were then submerged in PBS until the next measurement. The duration of the experiment was 14 days. The percentage of catalpol released was determined by calculating the ratio of the cumulative amount of catalpol released at each time point to the total cumulative released amount of catalpol at the end of the experiment.

2.4. In Vitro Cellular Experiments. *2.4.1. Cell Culture.* The cell line MC3T3-E1 was cultured in α-MEM supplemented with 10% fetal bovine serum (FBS) and 1% penicillin-streptomycin. The cells were maintained in a humidified environment at 37 °C and 5% CO_2. Prior to seeding MC3T3-E1 cells onto the substrate surface, the Ti substrates (including LBL, CAT-L, CAT-M, and CAT-H) were sterilized using γ radiation at a dose of 25 kGy emitted from cobalt-60. The Ti substrates were subsequently inoculated with MC3T3-E1 cells at a seeding density of 1×10^4 cells per well.

2.4.2. Cell Proliferation Assay. To assess cell viability and proliferation, the CCK-8 assay was utilized. The quantity of this dye correlates closely with the number of viable cells and their growth rate. Fourteen days after the cells were seeded onto the titanium substrates, the CCK-8 Cell Proliferation Cytotoxicity Assay Kit was used to evaluate cell proliferation. The absorbance of the CCK-8 solution under each experimental condition was measured at 450 nm using a Multiskan FC Microplate Photometer.

2.4.3. In Vitro Osteogenic Differentiation of MC3T3-E1 Cells on Ti Substrates. MC3T3-E1 cells, planted on Ti substrates, were cultured in complete α-MEM enriched with 0.1 μM dexamethasone, 50 μM ascorbic acid, and 10 mM β-glycerophosphate to induce osteogenic differentiation for 14 days. The osteogenic induction medium was refreshed every 2 days. Following a 14-day cultivation period, alkaline phosphatase (ALP) activity was assessed using an ALP staining kit.

2.4.4. Western Blot Analysis. Following 14 days of incubation, proteins were extracted from the cells cultured on the surface of titanium plates using radio-Immunoprecipitation Assay (RIPA) buffer (Solarbio, China) containing 1% phenylmethylsulfonyl fluoride (Solarbio, China) and phosphatase inhibitor (Beyotime Biotechnology, China). Protein concentrations were determined using a bicinchoninic acid assay according to the manufacturer's protocol (Beyotime Biotechnology). Protein samples were subsequently denatured by boiling at 95 °C for 5 min and then 30 μg of proteins was resolved on 10% sodium dodecyl sulfate−polyacrylamide gel electrophoresis (SDS-PAGE) gel. Separated proteins were electroblotted onto poly(vinylidene fluoride) (PVDF) membranes overnight at 4 °C. The membranes were blocked for 1 h with 5% skim-milk in tris-buffered saline (TBST) (0.1% Tween 20 in Tris-buffered saline) and incubated for 10−12 h at 4 °C with primary antibodies specific for COL1 (1:500 dilution; Wanleibio, China), OCN (1:1000 dilution; Cell Signaling Technology), RUNX2 (1:1000 dilution; Cell Signaling Technology), β-Actin (1:2000 dilution; Servicebio Technology, China). After extensive washed with TBST, membranes were incubated with appropriate horseradish peroxidase-conjugated secondary antibodies (1:1000 dilution) for 1 h at room temperature. The immunoreactivity of protein-antibody complexes was detected and imaged following exposure to enhanced chemiluminescence (ECL) substrate on a gel image-processing system.

2.5. In Vivo Experiments in Animals. *2.5.1. Ethical Statements and Laboratory Animals.* All animal experiments were approved and strictly adhered to the institutional standards for animal care under the supervision and guidance of the Animal Research Ethics Committee of Wenzhou Medical University. Healthy male Sprague−Dawley rats (250−300 g)

https://doi.org/10.1021/acsomega.4c02322
ACS Omega 2024, 9, 29544−29556

were purchased from Wenzhou Medical University (license no. SCXK[ZJ]2005-0019). All animal care and use conformed to the Guide for the Care and Use of Laboratory Animals of the Chinese National Institutes of Health and the work was approved by the Animal Care and Use Committee of Wenzhou Medical University (wydw2012-0079).

2.5.2. Animal Model of Osteoporosis. The study used 40 three-month-old female Sprague−Dawley rats that underwent a week of environmental adaptation before the start of the experiment. According to previous studies,[31] these rats underwent bilateral oophorectomy. Post-surgery, they were housed in pathogen-free isolation cages with four rats per cage. The cages were maintained under a 12 h light/dark cycle, with environmental temperatures controlled at 22−24 °C and humidity maintained at 50−55%. Each animal underwent a 7-day acclimatization period before participating in the experiments.

2.5.3. Implantation of Ti Substrates into the Femoral Intramedullary. Following the previously mentioned procedure, ovariectomized (OVX) rats underwent femoral intramedullary implantation of Ti substrates.[32] The process began with the administration of pentobarbital sodium via intraperitoneal injection for anesthesia, administered at 50 mg/kg of body weight. To prepare for surgery, we shaved and disinfected the hair on the hind legs of the rats using 75% alcohol. Subsequently, an incision was made on the inner side of the hind legs to expose the outer side of the knee joint. Next, a passage with a diameter of 2 mm was drilled along the femoral shaft axis originating from the patellofemoral groove located at the distal end of the femur. Sterilized Ti rods, either coated or uncoated with various concentrations of catalpol in the LBL, were placed into the medullary cavity through the created channel. The joint was then sutured layer by layer, and all rats were placed in a controlled environment within the animal care laboratory. For prophylaxis, the animals received daily intramuscular injections of cefazolin (10 mg/kg) for three consecutive days following the surgery. And immobilization was not applied to the operated area. Rats were divided into four groups based on the surface treatment of the titanium rods: unlayered titanium rods (control group), titanium rods layered with HA/CS, and titanium rods layered with catalpol at different concentrations (CAT-L, CAT-M, and CAT-H). At the second week after implantation of the titanium substrate, we euthanized the rats by overinjection of chloral hydrate and removed the femur.

2.5.4. Micro-Computed Tomography (CT) Evaluation. The resected femurs were cleared of surrounding soft tissues and fixed in 4% formaldehyde solution at a low temperature (4 °C) for 48 h. We then analyzed these fixed femoral samples in detail using a Scanco μCT 100 high-definition micro-CT scanner. For image acquisition, we set the voltage to 70 kV and the current to 114 μA, which ensured an isotropic voxel resolution of 10 μm. To distinguish bones from other tissues or structures, we used a multilevel thresholding method, where the threshold was set to 205 for bones and 700 for implants, and performed 3D reconstruction and quantitative evaluation using a specialized software. The region of interest (VOI) was defined as the cancellous bone from 2 mm beneath the peak of the epiphyseal plate to 100 slices toward the distal end of the epiphyseal plate. We also calculated a number of morphological parameters, including the ratio of bone volume to tissue volume (BV/TV), the amount of cancellous bone (Tb.N, per millimeter), the thickness of cancellous bone (Tb.Th, micrometers), the spacing of the cancellous bone (Tb.Sp, mm), the joint density (Conn.D, per cubic millimeter), and the bone mineral density (BMD, milligrams/HA/cubic centimeter).

2.5.5. Histological and Immunohistochemical Analyses. After completion of the micro-CT scans, all femoral samples were decalcified using a 10% ethylenediaminetetraacetic acid (EDTA) solution at a low temperature (4 °C) for 8 weeks. Subsequently, the implanted titanium material was carefully removed from the interior of the femur along its axis. The removed bone tissue was progressively dehydrated with different concentrations of ethanol and embedded in wax for meticulous ultrathin sectioning. Longitudinal sections with a thickness of 5 μm were prepared and processed for hematoxylin and eosin (H&E) and Masson's trichrome staining. Stained tissue slices were photographed using a light microscope fitted with a digital camera. The results were expressed as bone area (BA %), which was defined as the area percentage of newly formed bone divided by the area of defect extending 100 μm from the implant surface.[11,33]

For immunohistochemical staining, the sections were dewaxed in xylene, rehydrated in different concentrations of ethanol, and treated with 3% hydrogen peroxide to eliminate endogenous peroxidase activity. For antigen recovery, sections were boiled in a solution containing 10 mM sodium citrate (pH 6.0) for 30 min. Next, they were blocked using 10% normal goat serum for 15 min at room temperature and incubated overnight at 4 °C in a humid environment using primary antibodies against RUNX2 and OCN at a dilution of 1:100. After adequate washing with PBS, the sections were incubated at room temperature with the corresponding secondary antibodies for 1 h for final immunoreactivity detection using DAB.

2.6. Statistical Analyses. The results presented in this study were based on the mean ± standard deviation (SD) derived from a minimum of three separate experiments. For statistical processing of the data, we utilized SPSS 18.0 statistical analysis software (IBM Corporation). Graphical representation of the data was accomplished using GraphPad Prism software (San Diego, California). To assess the significance of the differences between various experimental groups, we applied the unpaired Student's *t*-test or one-way analysis of variance (ANOVA), complemented by post-analysis using Tukey's honest significance test. In this study, differences were considered statistically significant when the p-value was less than 0.05.

3. RESULT

3.1. Surface Characterization of Ti Substrates. Fourier transform infrared spectroscopy (FTIR) analysis was used to verify whether catalpol effectively binds to the CS multilayers. Table 1 shows the attribution of bands for the major chemical bonds in PEI, HA, CS, and CAT analyzed by FTIR spectroscopy in ATR mode. From the chemical structure of catalpol in Figure

Table 1. Attribution of the Main Bands of PEI, HA, CS, and CAT Analyzed by FTIR in ATR Mode

chemical bonds	wavenumber (cm^{-1})	corresponding chemicals
V_{N-H}	3312	PEI and CS
V_{O-H}	3440	HA, CS, and CAT
V_{C-H}	2915	PEI, HA, and CS
V_{C-O-C} ring mode	1089	HA, CS, and CAT
V_{C-O^-} ($-COO^-$)	1591	HA
$V_{C=C}$	1715	CAT

https://doi.org/10.1021/acsomega.4c02322
ACS Omega 2024, 9, 29544−29556

2a, we can see that catalpol is rich in hydroxyl, ether ring structure. Comparing with Table 1, we can know that the

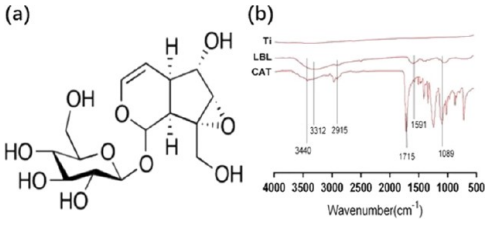

Figure 2. Analyzing surface chemical composition using FTIR. (a) Chemical structure of catalpol. (b) FTIR wide scan spectra of Ti; LBL, Ti-PEI coated with a multilayer of HA-CS; CAT, Ti-PEI coated with a multilayer of HA-CS with catalpol immobilization.

absorption peaks of hydroxyl group and ether ring are at 3440 and 1089 cm^{-1}, respectively. Figure 2b shows the FTIR spectra of pure titanium, LBL-treated, and CAT-treated substrates. Pure titanium and the substrate did not show any significant absorption peaks in the measurement range of 500−4000 cm^{-1}. However, a faint absorption peak at 3312 cm^{-1} suggests that the PEI layer contains a tertiary amine structure. Broad peaks at 3440 and 1089 cm^{-1} indicate that the surface is enriched with hydroxyl and ether ring structures, respectively, which are characteristic of HA/CS coatings. The 1591 cm^{-1} peak shows the presence of carboxyl groups in the sodium hyaluronate. The 1715 cm^{-1} peak indicates a carbon−carbon double-bond structure. FTIR analysis results confirmed the successful conjugation of HA/CS-Catalpol multilayer coating on Ti-PEI substrate.

The surface structure of the titanium substrate was carefully analyzed using a scanning electron microscope. Figure 3a shows the exterior layer of the pure titanium substrate, which exhibits a relatively smooth and uniform texture in contrast to the rough streaked surface of the PEI-coated covered titanium substrate (Figure 3b). In addition, a Ti-PEI-HA substrate with a single layer of CS was added (Figure 3d), and its surface texture was similar to that of the Ti-PEI substrate, which showed a rough stripe-like appearance. However, the Ti-PEI-HA substrate (Figure 3c) and the Ti-PEI substrate were coated with multilayer HA/CS coatings (Figure 3e), showing similar smooth surface characteristics to those of the pure titanium substrate. Finally, as shown in Figure 3f, the catalytic phenol deposited on the exterior layer of the Ti-PEI-HA/CS substrate appeared in a monodisperse form with a rough appearance, indicating that the multilayer HA/CS catalytic phenol coating had been successfully formed on the exterior layer of the Ti-PEI-HA substrate.

The affinity of implants for water plays a crucial role in determining osteoblast adhesion, influencing biological activity, and facilitating bone conductivity. We tested the water contact angles of pure titanium, Ti-PEI, LBL, and three CAT variant (L, M, H) substrates. As shown in Figure 4, the application of PEI or

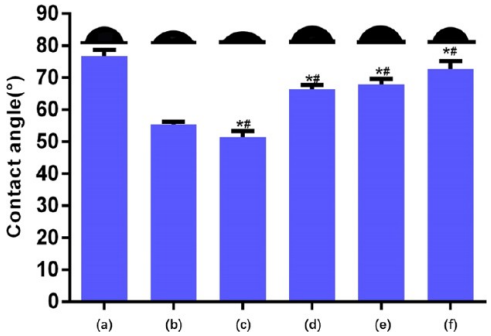

Figure 4. Water contact angles of different samples. (a) Ti; (b) Ti-PEI; (c) LBL; (d) CAT-L; (e) CAT-M; (f) CAT-H. Data have been presented as mean ± SD from three independent experiments ($n = 3$). * Statistically significant difference when compared to the Ti group. ($P < 0.05$). # Statistically significant difference when compared Ti-PEI group ($P < 0.05$).

PEI-HA/CS coatings to the titanium surface significantly reduced the water contact angle and improved its hydrophilicity compared with that of the pure titanium substrate. For example, the contact angle of titanium was reduced from 76.8 ± 1.8° to 55.3 ± 1.1° after the PEI coating treatment and further reduced to 51.4 ± 1.9° after further superimposition of the LBL layer on the Ti-PEI surface. The reduction in the contact angle, which is indicative of enhanced hydrophilicity, may be associated with the cationic amine groups present in CS. Notably, coating the catalytic phenol on the surface of the LBL substrate resulted in a dose-dependent increase in the water contact angle as compared to Ti-PEI or LBL substrates. The contact angles for CAT-L,

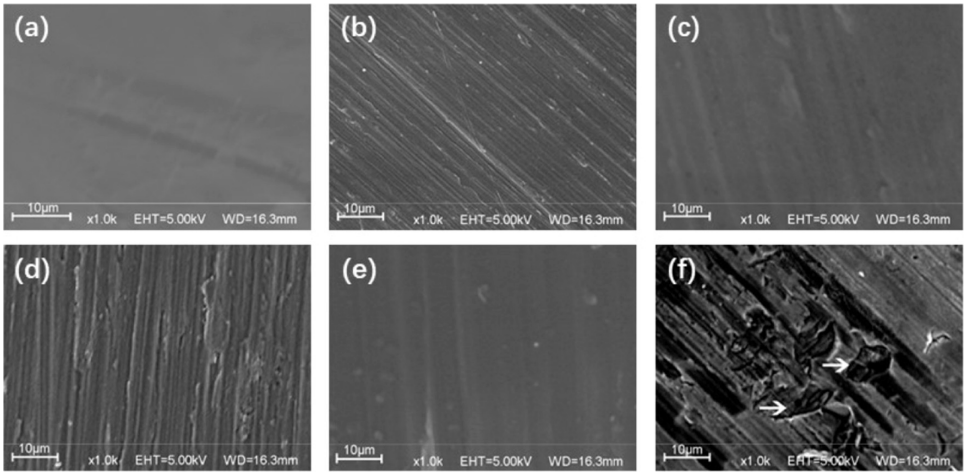

Figure 3. SEM photographs of different surfaces. SEM images of (a) pure Ti, (b) Ti-PEI, (c) Ti-PEI-HA, (d) Ti-PEI coated with monolayer HA-CS, (e) Ti-PEI coated with multilayer HA-CS, and (f) Ti-PEI coated with multilayer HA-CS with catalpol immobilization. The arrow indicates catalpol.

https://doi.org/10.1021/acsomega.4c02322
ACS Omega 2024, 9, 29544−29556

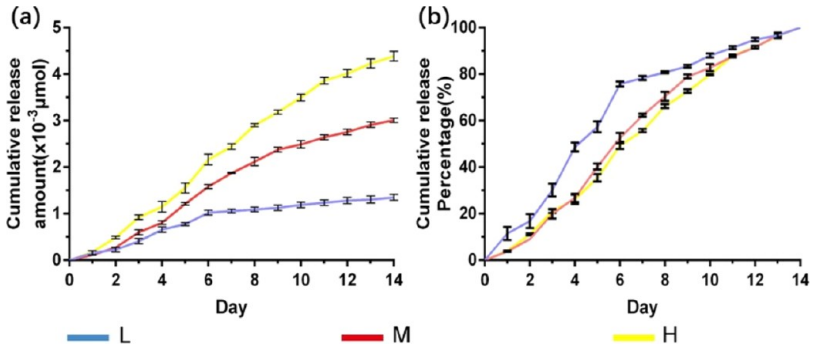

Figure 5. Release profiles of HA/CS multilayered surfaces with different levels of catalpol. An ultraviolet−visible dual-beam spectrophotometer was used to determine optical density (OD) to obtain (a) the total amount released over time and (b) accumulated release percentage. Data have been presented as mean ± SD from three independent experiments (n = 3).

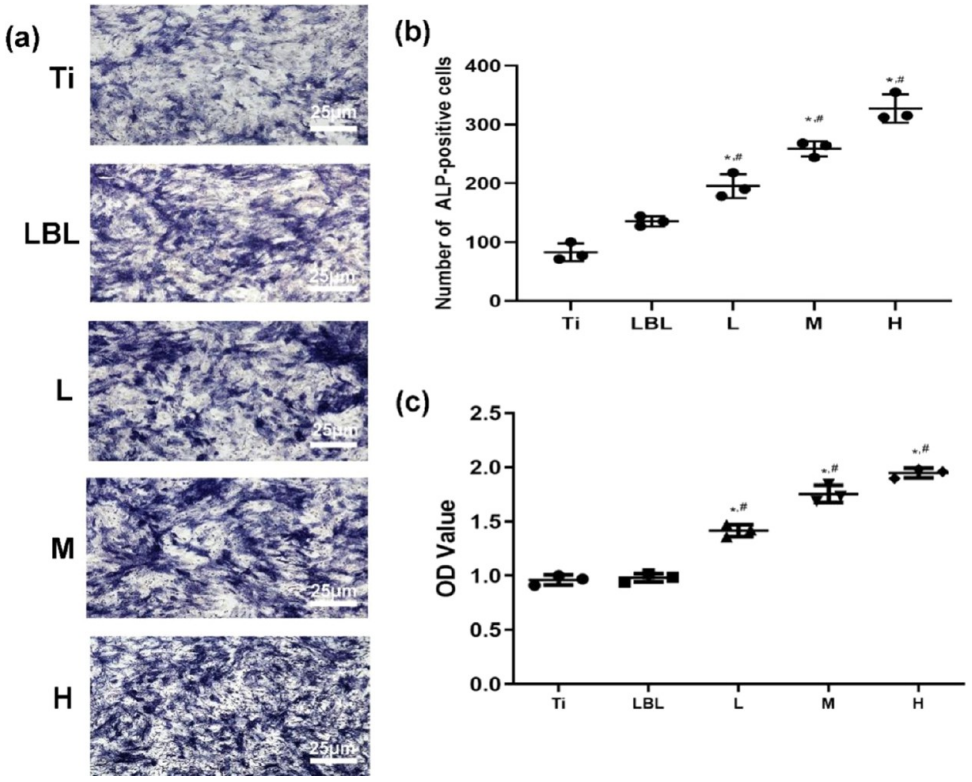

Figure 6. In vitro assessment of proliferation by CCK-8 assay, and osteogenic differentiation by ALP staining of MC3T3-E1 cells on different surfaces. (a, b) ALP activity (40×) and (c) CCK-8 assay. Data have been presented as mean ± SD from three independent experiments (n = 3). * Statistically significant difference compared to the Ti group (P < 0.05). # Statistically significant difference compared to the HA/CS multilayer group (P < 0.05). Data have been presented as mean ± SD from three independent experiments (n = 3).

CAT-M, and CAT-H were 66.4 ± 1.3°, 67.9 ± 1.7°, and 72.7 ± 2.4°. Although the water contact angle was superior to that of LBL substrates or Ti-PEI, the addition of catalpol led to lower contact angles than those of pure titanium substrates. Therefore, the immobilization of multilayer HA/CS-catalyzed phenol on titanium surfaces improves hydrophilicity, which is beneficial for cell adhesion.

3.2. In Vitro Catalpol Release Profile. Subsequently, we investigated the release pattern of catalpol from the HA/CS-CAT substrates over a 14-day period. Figure 5a shows the relationship between the cumulative release of catalpol and the initial catalpol concentration in the HA/CS catalpol coating. Specifically, the maximum release of catalpol was observed for the CAT-H substrate, and the minimum release was observed for CAT-L within 14 days, with the release from the CAT-M substrate lying in between. Within the first 6 days, the CAT-L substrate had a faster rate of catalpol release, reaching 80% (Figure 5b). In contrast, it took approximately 8 days for CAT-M or CAT-H substrates to release 80% of the catalpol. This suggests that the CAT-L substrate had a faster drug release rate, whereas the CAT-M and CAT-H substrates provided a more sustained drug release effect.

3.3. In Vitro Osteoblast Differentiation. We explored the effects of CAT substrate on the induction of bone formation. Figure 6b shows the ALP activity of the pure Ti, LBL, and CAT substrates. We found that ALP activity was differentially elevated on CAT substrates compared with pure Ti and LBL substrates, especially on HA/CS-H substrates. This finding suggests that cells cultured on CAT substrates have higher differentiation

https://doi.org/10.1021/acsomega.4c02322
ACS Omega 2024, 9, 29544−29556

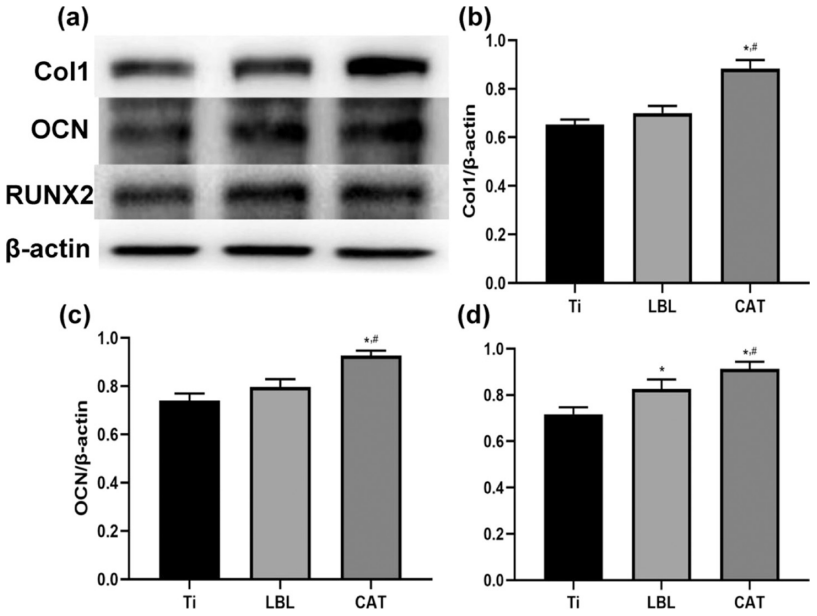

Figure 7. Effect of catalpol on the regulation of the Wnt/β-catenin signaling pathway in MC3T3-E1 cells. (a) Western blot analysis of Col1, OCN, and RUNX2 in MC3T3-E1 cells post-treatment of catalpol. (b−d) Percentage of Col1, OCN, and RUNX2 in MC3T3-E1 cells post-treatment of catalpol. * Statistical significance compared to the Ti group ($P < 0.05$). # Statistical significance compared to the LBL group ($P < 0.05$). Data have been presented as mean ± SD from three independent experiments ($n = 3$).

capacity. This suggests that catalpol has a positive effect on osteoblast precursor cell differentiation.

3.4. In Vitro MC3T3-E1 Cell Proliferation. The cells were cultured for 14 days on LBL-coated substrates that were free of catalpol or contained different concentrations of catalpol. Subsequently, we assessed the cell viability and proliferation. As demonstrated in Figure 6c, cells cultured on CAT substrates containing moderate to high concentrations of catalpol showed higher proliferation rates compared to cells cultured on HA/CS substrates only or on CAT substrates containing low concentrations of catalpol. This result implies that culturing cells on substrates with higher concentrations of catalpol is more favorable for cell proliferation.

3.5. In Vitro Osteogenic Protein Expression. The Wnt/β-catenin signaling pathway is one of the key pathways regulating osteoblast differentiation and bone formation.[34] With this in mind, we investigated the expression levels of key regulatory factors within MC3T3-E1 cells that had been cultivated on various substrates. As shown in Figure 7, the levels of Col1, OCN, and RUNX2 mRNA expression in the CAT group was significantly higher than that in the Ti group and the LBL group. Additionally, the LBL group demonstrated enhanced the expression levels of RUNX2, compared to the Ti-only group. Collectively, the results suggested that catalpol can promote the expression of osteogenic proteins via the Wnt/β-catenin pathway, and the application of a multilayered coating has potential to enhance this effect, suggesting a synergistic role in fostering osteoblast differentiation.

3.6. New Bone Formation and Osseointegration of the HA/CS-Catalpol Substrates. We assessed the in vivo bone induction capability of the LBL substrate (presented as Ti rods) either unloaded or loaded with catalpol using the OVX rat femoral medullary implantation model. Two weeks after substrate implantation, the rats were euthanized. Their femurs, which contained the implanted substrates, were analyzed using μCT (Figure 8). In contrast to both the uncoated pure titanium and LBL groups, a notable increase in bone volume around the implant was observed in the CAT groups, with the HA/CS-H group showing the most significant enhancement (Figure 8a). Detailed quantitative morphometric assessments of the bone volume fraction (BV/TV), bone mineral density (BMD), and related cancellous bone characteristics such as the number of trabeculae (Tb.N), spacing between trabeculae (Tb.Sp), trabecular thickness (Tb.Th), and trabecular connection density (Conn.D) around the implant revealed an increased formation of new bone in the HA/CS-catalpol substrate groups. Among these, the HH group demonstrated the strongest osteoinductive effect (Figure 8b−g).

Subsequently, histological evaluations were conducted to closely investigate the extent of new bone formation around the implant. After delicately extracting the Ti rods from the femur, the bone tissues underwent a decalcification process, subsequently, the bone tissue undergoes staining procedures using hematoxylin and eosin (H&E) (Figure 9a) as well as Masson's trichrome (Figure 9b). Different levels of newly formed bone were observed. In the control group, unmineralized connective tissue was observed around the Ti implant, as well as a scarcity of new bone formation. Conversely, the LBL groups displayed the formation of neo-trabecular bone and unmineralized bone matrix immediately next to the substrate, aligned with the μCT results. New bone formation in the CAT groups was more extensive than that in the LBL groups, with a large number of osteoblasts lining the newly formed bone (Figure 9c).

Finally, immunohistochemical staining for the osteogenic markers OCN (Figure 10a) and RUNX2 (Figure 10b) was performed, and immunohistochemical experiments showed strong positive immunoreactivity found in the cells of new bone formation in the CAT groups. This indicated increased osteoblast formation in the CAT group compared to the Ti group and the LBL group, which was positively correlated with the concentration. In conclusion, these results suggest that additional coating of catalpol on HA/CS substrates induces new bone formation and is more osteogenic than LBL or Ti substrates.

https://doi.org/10.1021/acsomega.4c02322
ACS Omega 2024, 9, 29544−29556

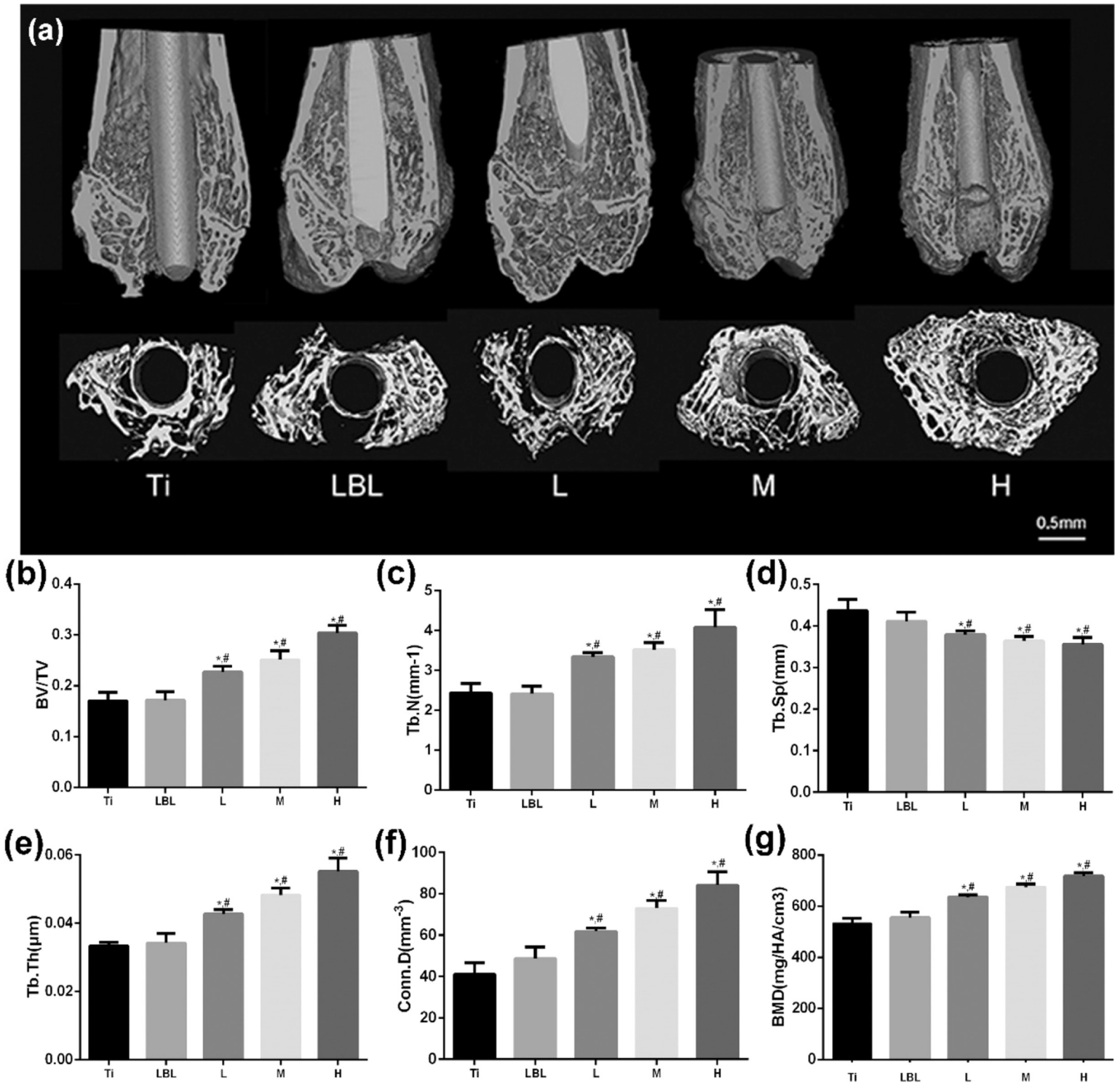

Figure 8. Reconstruction and quantitative micro-CT analysis of the distal femur 2 weeks after implantation. (a) 3D imaging showcasing the structure of the distal femur bone in both the Ti rats and Ti rats with varying concentrations of loaded catalpol. (b) Quantification analysis of bone volume per total volume (BV/TV), (c) number of trabeculae (Tb.N), (d) space between trabeculae (Tb.Sp), (e) thickness of trabeculae (Tb.Th), (f) density of trabecular connections (Conn.D), and (g) bone mineral density (BMD) for each group at 2 weeks. Data have been presented as mean ± SD from three rats per group (n = 3). * Statistically significant difference when compared to the Ti group (P < 0.05). # Statistically significant difference when compared to the HA/CS multilayer group (P < 0.05).

4. DISCUSSION

Titanium is currently the most commonly used material for internal implants[1] due of its excellent biocompatibility, non-inflammatory properties, and mechanical durability.[35] However, Ti itself is a bioinert material that lacks bioinductivity. Usually, Ti implants only provide early rigid fixation, whereas fracture healing mainly depends on the regenerative capacity of the bone itself.[36] In scenarios such as severe trauma, persistent infections, extensive resections of musculoskeletal tumors, or prior failures of implants, there can still be instances of unhealed bone or significant bone defects. Consequently, it is essential to perform functional modifications on the surface of the Ti substrate, primarily achieved through the assembly of coatings to realize surface functionalization. For instance, coatings impregnated with antibiotics are commonly employed to avert potential infections,[37] whereas coatings made from inorganic nonmetal materials are recognized for their ability to promote the process of osteointegration.[38] The techniques available for coating assembly are myriad and encompass advanced methods such as 3D printing,[39] sintering technology,[38] and biomimetic approaches.[40]

https://doi.org/10.1021/acsomega.4c02322
ACS Omega 2024, 9, 29544−29556

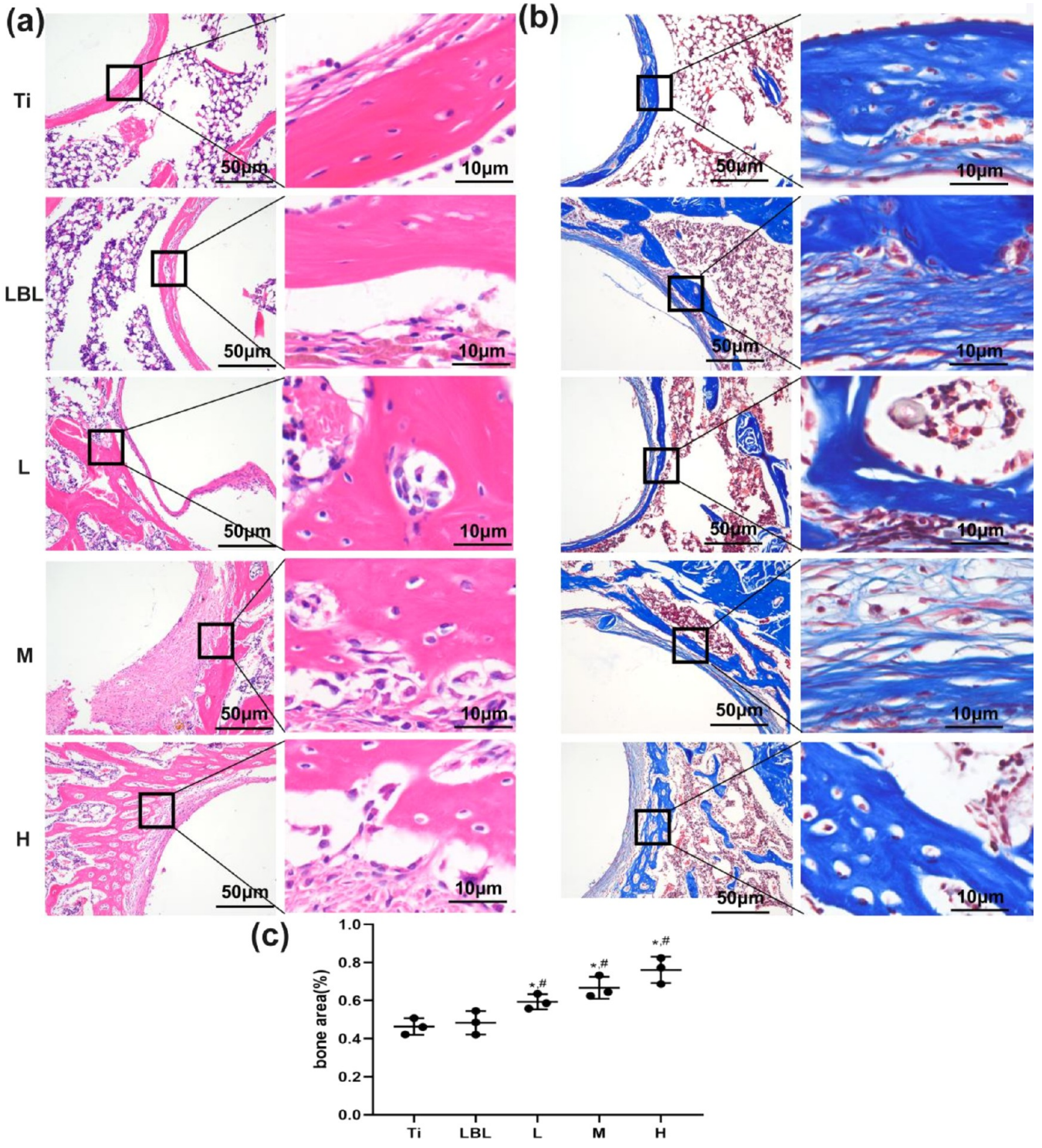

Figure 9. Examination of histological sections from the decalcified samples. (a) H&E staining. (b) Masson staining. Images in the right and left panels were magnified at 10× and 40×, respectively. (c) BA %. The analysis of histological morphology, using H&E staining conducted 2 weeks post-implantation, was quantitatively assessed in terms of bone area (BA %) and is depicted in (c). * Statistically significant difference when compared to the Ti group ($P < 0.05$). # Statistically significant difference when compared to the LBL group ($P < 0.05$). Data have been presented as mean ± SD from three rats per group ($n = 3$).

In this study, we established titanium substrate surface functionalization using catalpol via layer-by-layer technology. Catalpol is a natural iridoid glycoside that contains a cyclic iridoid core and side-chain glucose unit.[41] Catalpol presents numerous benefits as a promising agent for bone regeneration. First, its safety profile is well established. Derived and concentrated from the root of Rehmannia glutinosa, a plant with over 3000 years of clinical usage, catalpol has demonstrated no cytotoxic effects on a variety of cell types and negligible side effects in animal studies.[17,42] Moreover, it offers practical advantages due to its water solubility, ease of transport, and stability. Economically, catalpol is cost-effective and can be

https://doi.org/10.1021/acsomega.4c02322
ACS Omega 2024, 9, 29544−29556

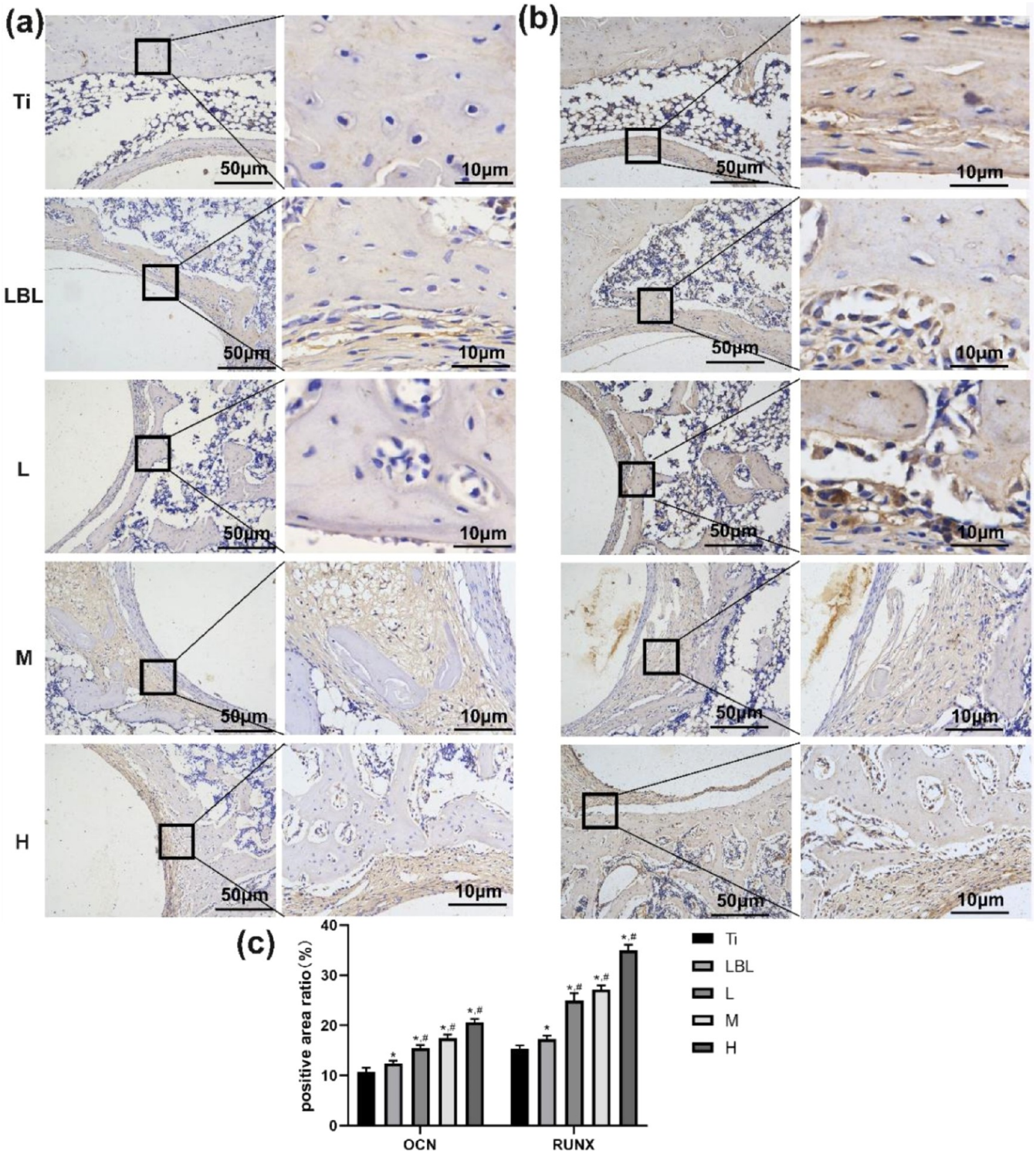

Figure 10. Immunohistochemical detection of OCN and RUNX2 expression levels around implants loaded with Ti, LBL, and different concentrations of catalpol. (a) OCN, (b) RUNX2. Images in the right and left panels were magnified at 10× and 40×, respectively. (c) Positive area ratio (%). * Statistically significant difference when compared to the Ti group ($P < 0.05$). # Statistically significant difference when compared to the LBL group ($P < 0.05$). Data have been presented as mean ± SD from three rats per group ($n = 3$).

efficiently extracted and isolated from Radix Rehmanniae.[43] Most notably, it has been shown to enhance bone mineralization. Overall, catalpol is an excellent candidate for bone-healing applications.

Bone remodeling occurs through a balanced interplay between osteoblast-led bone formation and osteoclast-driven bone resorption.[44] Osteoblasts are derived from BMSCs[23] and their differentiation is regulated by numerous factors, among which the Wnt/β-catenin pathway is crucial.[45] Various studies have shown that the addition of agonists of the Wnt/β-catenin pathway can increase systemic and focal bone formation,[25] making this pathway an attractive target for promoting bone regeneration.[34] Hence, it is anticipated that these bioactive molecules, capable of fostering an ideal osteogenic micro-

https://doi.org/10.1021/acsomega.4c02322
ACS Omega 2024, 9, 29544−29556

environment for bone marrow-derived mesenchymal stem cells (BMSCs), will expedite the process of bone formation in prospective clinical applications.[46] Some studies have demonstrated that catalpol could significantly enhance the bone-healing capacity of BMSCs through the Wnt/β-catenin pathway and promote osteogenesis.[21] The interaction between Wnt ligands and Frizzled, along with LRP 5/6 receptors, results in the suppression of GSK-3β activity and the stabilization of β-catenin. Subsequently, β-catenin relocates to the nucleus, where it binds to the N-terminus of DNA-binding proteins from the Tcf/Lef family, thereby orchestrating the transcriptional regulation of osteoblastogenesis-related target genes, such as Runx2 and Osterix.[23] In the present study, the results showed that the presence of catalpol promoted significant expression of proteins and growth factors related to the Wnt/β-Catenin pathway, Runx2, and OCN in the catalpol-loaded Ti substrate groups. Moreover, the multiplication and osteogenesis induction of MCTC3-E1 cells in the medium containing catalpol were obviously higher than those in the control group without catalpol. The above experimental results were positively correlated with the drug-loading concentration of the Ti substrates in vitro. In summary, sustained release of catalpol on the surface of Ti is beneficial for creating a local microenvironment to stimulate osteogenesis. We used SD rats to investigate the effects of catalpol-loaded titanium implants in vivo. Compared to the unmodified titanium matrix and uncoated titanium substrate, the findings also demonstrated that the local release of catalpol could stimulate early bone formation and increase bone mineral density. The effect of high catalpol concentrations was the most obvious. At the same time, there were no obvious side effects in animal models.

The studies have highlighted that elevating the surface roughness of titanium implants can substantially bolster their initial stability and further the integration with bone tissue,[47] an enhancement evident across micro- and nanoscale roughness levels.[48] Importantly, this augmentation of surface roughness does not detrimentally affect the initial adhesion and the lateral expansion of osteoblasts.[48] The strategies to enhance the surface roughness encompass a variety of techniques, such as the utilization of abrasion methods and the application of ceramic-based coatings.[49] It is a fundamental concept that the surface modification of titanium implants inherently remodels the roughness profile. In our investigation, we fabricated a biomimetic coating on the surface of titanium implants by LBL technique, resulting in a marked increase in surface roughness, as confirmed by SEM analysis. Partial in vitro and in vivo analyses have demonstrated superior osseointegration around the titanium implants adorned with the multilayered coating. These results have not only corroborated the positive influence of surface roughness on osseointegration but also steered our research toward innovative approaches in the domain of biomimetic coating-induced osseointegration.

This study had several limitations. First, as mentioned above, the molecular process of catalpol osteogenesis has not yet been fully elucidated. Second, we believe that there is an optimal drug-loading concentration that needs to be further determined. Third, the multilayer composition of catalpol loaded with catalpol has not yet been studied in detail. Therefore, future research should focus on the development of the best coating materials, clear drug concentration, and understanding the specific mechanism of catalpol action.

5. CONCLUSIONS

In this study, we successfully formed HA/CS multilayer films using layer-by-layer technology, loaded catalpol on a Ti substrate, and achieved continuous and controlled release. The results showed that the controlled release of catalpol promoted the proliferation and differentiation of osteoblasts and enhanced osteogenesis during the early period of culture. In addition, implants coated with catalpol can also increase early bone integration and bone formation in vivo and establish stability in the early stage. This study provides a new, eco-friendly, and convenient method for the functionalization of Ti substrate surfaces and is helpful for the development of new implants.

■ ASSOCIATED CONTENT

Data Availability Statement

The present study incorporates data sourced from an external entity, with the visual data derived from animal studies having been amassed by an external organization. As per our arrangement with the proprietor of the data, we are constrained from divulging such information. Nonetheless, the manuscript encompasses a trove of original data that is eligible for disclosure as per the terms of our agreement.

■ AUTHOR INFORMATION

Corresponding Author

Jiahao Tang − *Department of Orthopaedics Surgery, The Second Affiliated Hospital and Yuying Children's Hospital of Wenzhou Medical University, Wenzhou 325000 Zhejiang Province, People's Republic of China; Key Laboratory of Orthopedics of Zhejiang Province, Department of Orthopedics, The Second Affiliated Hospital and Yuying Children's Hospital of Wenzhou Medical University, Wenzhou 325000 Zhejiang Province, People's Republic of China;* orcid.org/0009-0008-9114-3504; Email: feygktjh@126.com

Authors

Jiayi Yang − *Department of Obstetrics and Gynecology, The First Affiliated Hospital Hospital of Wenzhou Medical University, Wenzhou 325000 Zhejiang Province, People's Republic of China*

Wei Zhang − *Department of Orthopaedics Surgery, The Second Affiliated Hospital and Yuying Children's Hospital of Wenzhou Medical University, Wenzhou 325000 Zhejiang Province, People's Republic of China; Key Laboratory of Orthopedics of Zhejiang Province, Department of Orthopedics, The Second Affiliated Hospital and Yuying Children's Hospital of Wenzhou Medical University, Wenzhou 325000 Zhejiang Province, People's Republic of China*

Binghao Lin − *Department of Orthopaedics Surgery, The Second Affiliated Hospital and Yuying Children's Hospital of Wenzhou Medical University, Wenzhou 325000 Zhejiang Province, People's Republic of China; Key Laboratory of Orthopedics of Zhejiang Province, Department of Orthopedics, The Second Affiliated Hospital and Yuying Children's Hospital of Wenzhou Medical University, Wenzhou 325000 Zhejiang Province, People's Republic of China*

Shuming Mao − *Department of Orthopaedics Surgery, The Second Affiliated Hospital and Yuying Children's Hospital of Wenzhou Medical University, Wenzhou 325000 Zhejiang Province, People's Republic of China; Key Laboratory of Orthopedics of Zhejiang Province, Department of Orthopedics, The Second Affiliated Hospital and Yuying Children's Hospital*

https://doi.org/10.1021/acsomega.4c02322
ACS Omega 2024, 9, 29544−29556

of Wenzhou Medical University, Wenzhou 325000 Zhejiang Province, People's Republic of China

Guangyao Liu − *Department of Orthopaedics Surgery, The Second Affiliated Hospital and Yuying Children's Hospital of Wenzhou Medical University, Wenzhou 325000 Zhejiang Province, People's Republic of China; Key Laboratory of Orthopedics of Zhejiang Province, Department of Orthopedics, The Second Affiliated Hospital and Yuying Children's Hospital of Wenzhou Medical University, Wenzhou 325000 Zhejiang Province, People's Republic of China*

Kai Tan − *Department of Orthopaedics Surgery, The Second Affiliated Hospital and Yuying Children's Hospital of Wenzhou Medical University, Wenzhou 325000 Zhejiang Province, People's Republic of China; Key Laboratory of Orthopedics of Zhejiang Province, Department of Orthopedics, The Second Affiliated Hospital and Yuying Children's Hospital of Wenzhou Medical University, Wenzhou 325000 Zhejiang Province, People's Republic of China*

Complete contact information is available at: https://pubs.acs.org/10.1021/acsomega.4c02322

Author Contributions

[‖]J.Y. and W.Z. contributed equally to this work.

Notes

The authors declare no competing financial interest.

■ ACKNOWLEDGMENTS

This work was funded by the Natural Science Foundation of Zhejiang Province (TGY24H060028), the Traditional Chinese Medicine of Zhejiang Province Science and Technology plan project (no. 2023010569), and Wenzhou Municipal Science and Technology Bureau (nos. 2023ZM0037 and 2021Y0444).

■ REFERENCES

(1) Adell, R.; Eriksson, B.; Lekholm, U.; Brånemark, P. I.; Jemt, T. Long-term follow-up study of osseointegrated implants in the treatment of totally edentulous jaws. *Int. J. Oral Maxillofac. Implants* **1990**, *5*, 347−359.

(2) García-Alonso, M.; Saldaña, L.; Vallés, G.; González-Carrasco, J. L.; González-Cabrero, J.; Martínez, M. E.; Gil-Garay, E.; Munuera, L. In vitro corrosion behaviour and osteoblast response of thermally oxidised Ti6Al4V alloy. *Biomaterials* **2003**, *24*, 19−26.

(3) Zhu, Y.; Kong, B.; Liu, R.; Zhao, Y. Developing biomedical engineering technologies for reproductive medicine. *Smart Med.* **2022**, *1*, No. e20220006, DOI: 10.1002/SMMD.20220006.

(4) Li, C.; Cui, W. 3D bioprinting of cell-laden constructs for regenerative medicine. *Eng. Regener.* **2021**, *2*, 195−205.

(5) Sundfeldt, M.; Carlsson, L. V.; Johansson, C. B.; Thomsen, P.; Gretzer, C. Aseptic loosening, not only a question of wear: a review of different theories. *Acta Orthop.* **2006**, *77*, 177−197.

(6) Cordeiro, E. N.; Costa, R. C.; Carazzato, J. G.; Silva, J. d. S. Periprosthetic fractures in patients with total knee arthroplasties. *Clin. Orthop. Relat. Res.* **1990**, *252*, 182−189.

(7) Yoo, J. D.; Kim, N. K. Periprosthetic fractures following total knee arthroplasty. *Knee Surg Relat Res.* **2015**, *27*, 1−9.

(8) Chen, Z.; Cai, Z.; Zhuang, P.; Li, F.; Cui, W.; Li, Z. Living probiotic biomaterials for osteoporosis therapy. *Biomed. Technol.* **2023**, *1*, 52−64.

(9) Zhu, X.; Zhang, H.; Zhang, X.; Ning, C.; Wang, Y. In vitro study on the osteogenesis enhancement effect of BMP-2 incorporated biomimetic apatite coating on titanium surfaces. *Dental Mater. J.* **2017**, *36*, 677−685.

(10) Shyngys, M.; Ren, J.; Liang, X.; Miao, J.; Blocki, A.; Beyer, S. Metal-Organic Framework (MOF)-Based Biomaterials for Tissue Engineering and Regenerative Medicine. *Front. Bioeng. Biotechnol.* **2021**, *9*, No. 603608.

(11) Song, Y.; Ma, A.; Ning, J.; Zhong, X.; Zhang, Q.; Zhang, X.; Hong, G.; Li, Y.; Sasaki, K.; Li, C. Loading icariin on titanium surfaces by phase-transited lysozyme priming and layer-by-layer self-assembly of hyaluronic acid/chitosan to improve surface osteogenesis ability. *Int. J. Nanomed.* **2018**, *13*, 6751−6767.

(12) Li, T.; Tong, Z.; Gao, B.; Li, Y. C.; Smyth, A.; Bayabil, H. K. Polyethyleneimine-modified biochar for enhanced phosphate adsorption. *Environ. Sci. Pollut. Res.* **2020**, *27*, 7420−7429.

(13) Fahira, A. I.; Amalia, R.; Barliana, M. I.; Gatera, V. A.; Abdulah, R. Polyethyleneimine (PEI) as a Polymer-Based Co-Delivery System for Breast Cancer Therapy. *Breast Cancer* **2022**, *14*, 71−83.

(14) Han, S.-E.; Kang, H.; Shim, G. Y.; Kim, S. J.; Choi, H.-G.; Kim, J.; Hahn, S. K.; Oh, Y.-K. Cationic derivatives of biocompatible hyaluronic acids for delivery of siRNA and antisense oligonucleotides. *J. Drug Targeting* **2009**, *17*, 123−132.

(15) Udalamaththa, V. L.; Jayasinghe, C. D.; Udagama, P. V. Potential role of herbal remedies in stem cell therapy: proliferation and differentiation of human mesenchymal stromal cells. *Stem Cell Res. Ther.* **2016**, *7*, 110.

(16) Jiang, B.; Liu, J. H.; Bao, Y. M.; An, L. J. Catalpol inhibits apoptosis in hydrogen peroxide-induced PC12 cells by preventing cytochrome c release and inactivating of caspase cascade. *Toxicon* **2004**, *43*, 53−59.

(17) Zheng, X.-W.; Yang, W.-T.; Chen, S.; Xu, Q.-Q.; Shan, C.-S.; Zheng, G.-Q.; Ruan, J.-C. Neuroprotection of Catalpol for Experimental Acute Focal Ischemic Stroke: Preclinical Evidence and Possible Mechanisms of Antioxidation, Anti-Inflammation, and Antiapoptosis. *Oxid. Med. Cell. Longevity* **2017**, *2017*, No. 5058609.

(18) Liu, C.; Ma, R.; Wang, L.; Zhu, R.; Liu, H.; Guo, Y.; Zhao, B.; Zhao, S.; Tang, J.; Li, Y.; Niu, J.; Fu, M.; Zhang, D.; Gao, S. Rehmanniae Radix in osteoporosis: A review of traditional Chinese medicinal uses, phytochemistry, pharmacokinetics and pharmacology. *J. Ethnopharmacol.* **2017**, *198*, 351−362.

(19) Li, Y.; Chen, Q.; Sun, H.-J.; Zhang, J.-H.; Liu, X. The Active Ingredient Catalpol in Rehmannia glutinosa Reduces Blood Glucose in Diabetic Rats via the AMPK Pathway. *Diabetes, Metab. Syndr. Obes.: Targets Ther.* **2024**, *17*, 1761−1767.

(20) Zhang, M.-F.; Wang, J.-H.; Sun, S.; Xu, Y.-T.; Wan, D.; Feng, S.; Tian, Z.; Zhu, H.-F. Catalpol attenuates ischemic stroke by promoting neurogenesis and angiogenesis via the SDF-1α/CXCR4 pathway. *Phytomedicine* **2024**, *128*, No. 155362.

(21) Zhu, Y.; Wang, Y.; Jia, Y.; Xu, J.; Chai, Y. Catalpol promotes the osteogenic differentiation of bone marrow mesenchymal stem cells via the Wnt/β-catenin pathway. *Stem Cell Res. Ther.* **2019**, *10*, 37.

(22) Choi, E. M.; Suh, K. S.; Jung, W.-W.; Yun, S.; Park, S. Y.; Chin, S. O.; Rhee, S. Y.; Chon, S. Catalpol protects against 2,3,7,8-tetrachlorodibenzo-p-dioxin-induced cytotoxicity in osteoblastic MC3T3-E1 cells. *J. Appl. Toxicol.* **2019**, *39*, 1710−1719.

(23) Canalis, E. Management of endocrine disease: Novel anabolic treatments for osteoporosis. *Eur. J. Endocrinol.* **2018**, *178*, R33−R44.

(24) Zhu, H.; Wang, Y.; Liu, Z.; Wang, J.; Wan, D.; Feng, S.; Yang, X.; Wang, T. Antidiabetic and antioxidant effects of catalpol extracted from Rehmannia glutinosa (Di Huang) on rat diabetes induced by streptozotocin and high-fat, high-sugar feed. *Chin. Med.* **2016**, *11*, 25.

(25) Krishnan, V.; Bryant, H. U.; Macdougald, O. A. Regulation of bone mass by Wnt signaling. *J. Clin. Invest.* **2006**, *116*, 1202−1209.

(26) Lai, N.; Zhang, J.; Ma, X.; Wang, B.; Miao, X.; Wang, Z.; Guo, Y.; Wang, L.; Yao, C.; Li, X.; Jiang, G. Regulatory Effect of Catalpol on Th1/Th2 cells in Mice with Bone Loss Induced by Estrogen Deficiency. *Am. J. Reprod. Immunol.* **2015**, *74*, 487−498.

(27) Smith, R. C.; Riollano, M.; Leung, A.; Hammond, P. T. Layer-by-layer platform technology for small-molecule delivery. *Angew. Chem., Int. Ed.* **2009**, *48*, 8974−8977.

(28) Chen, J.; Pan, P.; Zhang, Y.; Zhong, S.; Zhang, Q. Preparation of chitosan/nano hydroxyapatite organic-inorganic hybrid microspheres for bone repair. *Colloids Surf. B* **2015**, *134*, 401−407.

(29) Pitt, W. G.; Morris, R. N.; Mason, M. L.; Hall, M. W.; Luo, Y.; Prestwich, G. D. Attachment of hyaluronan to metallic surfaces. *J. Biomed. Mater. Res., Part A* **2004**, *68*, 95−106.
(30) Arpornmaeklong, P.; Suwatwirote, N.; Pripatnanont, P.; Oungbho, K. Growth and differentiation of mouse osteoblasts on chitosan-collagen sponges. *Int. J. Oral Maxillofac. Surg.* **2007**, *36*, 328−337.
(31) Tao, Z.-S.; Zhou, W.-S.; Tu, K.; Huang, Z.-L.; Zhou, Q.; Sun, T.; Lv, Y.-X.; Cui, W.; Yang, L. The effects of combined human parathyroid hormone (1−34) and simvastatin treatment on osseous integration of hydroxyapatite-coated titanium implants in the femur of ovariectomized rats. *Injury* **2015**, *46*, 2164−2169.
(32) Tang, J.; Chen, L.; Yan, D.; Shen, Z.; Wang, B.; Weng, S.; Wu, Z.; Xie, Z.; Shao, J.; Yang, L.; Shen, L. Surface Functionalization with Proanthocyanidins Provides an Anti-Oxidant Defense Mechanism That Improves the Long-Term Stability and Osteogenesis of Titanium Implants. *Int. J. Nanomed.* **2020**, *15*, 1643−1659.
(33) Gao, Y.; Luo, E.; Hu, J.; Xue, J.; Zhu, S.; Li, J. Effect of combined local treatment with zoledronic acid and basic fibroblast growth factor on implant fixation in ovariectomized rats. *Bone* **2009**, *44*, 225−232.
(34) Hoeppner, L. H.; Secreto, F. J.; Westendorf, J. J. Wnt signaling as a therapeutic target for bone diseases. *Expert Opin. Ther. Targets* **2009**, *13*, 485−496.
(35) Mavrogenis, A. F.; Dimitriou, R.; Parvizi, J.; Babis, G. C. Biology of implant osseointegration. *J. Musculoskeletal Neuronal Interact.* **2009**, *9*, 61−71.
(36) Wernike, E.; Hofstetter, W.; Liu, Y.; Wu, G.; Sebald, H.-J.; Wismeijer, D.; Hunziker, E. B.; Siebenrock, K.-A.; Klenke, F. M. Long-term cell-mediated protein release from calcium phosphate ceramics. *J. Biomed. Mater. Res., Part A* **2010**, *92*, 463−474.
(37) Chen, F.; Skelly, J. D.; Chang, S.-Y.; Song, J. Triggered Release of Ampicillin from Metallic Implant Coatings for Combating Periprosthetic Infections. *ACS Appl. Mater. Interfaces* **2024**, *16*, 24421.
(38) Jose, S. M.; Rajaraman, V.; Ariga, P.; Ganapathy, D.; Sekaran, S. Analyzing the Surface Topography of Hafnium Nitride Coating on Titanium Screws: An In Vitro Analysis. *Cureus* **2024**, *16*, No. e57385.
(39) Li, Z.; Jin, L.; Yang, X.; Liu, H.; Qian, S.; Wang, Z.; Liu, J.; Wang, J.; Chen, J.; Su, B.; Peng, C.; Wang, J.; Shi, Z. A multifunctional ionic liquid coating on 3D-Printed prostheses: Combating infection, promoting osseointegration. *Mater. Today Bio* **2024**, *26*, No. 101076.
(40) Zhang, Y.; Zhang, J.; Sun, B.; Ma, L.; Ma, Y. Catalpol Promotes Osseointegration of Titanium Implants under Conditions of Type 2 Diabetes via AKT/GSK3β/FYN Pathway-Mediated NRF2 Activation. *ACS Omega* **2024**, *9*, 5761−5771.
(41) Dvorkin, L.; Song, K. Y. Herbs for benign prostatic hyperplasia. *Ann. Pharmacother.* **2002**, *36*, 1443−1452.
(42) Jiang, B.; Shen, R. F.; Bi, J.; Tian, X. S.; Hinchliffe, T.; Xia, Y. Catalpol: a potential therapeutic for neurodegenerative diseases. *Curr. Med. Chem.* **2015**, *22*, 1278−1291.
(43) Lin, C.; Lu, Y.; Yan, X.; Wu, X.; Kuai, M.; Sun, X.; Chen, Q.; Kong, X.; Liu, Z.; Tang, Y.; Jing, Y.; Li, Y.; Zhang, Q.; Bian, H. Catalpol protects glucose-deprived rat embryonic cardiac cells by inducing mitophagy and modulating estrogen receptor. *Biomed. Pharmacother.* **2017**, *89*, 973−982.
(44) Ikeda, K.; Takeshita, S. Factors and mechanisms involved in the coupling from bone resorption to formation: how osteoclasts talk to osteoblasts. *J. Bone Metab.* **2014**, *21*, 163−167.
(45) Rudnicki, M. A.; Williams, B. O. Wnt signaling in bone and muscle. *Bone* **2015**, *80*, 60−66.
(46) Garg, P.; Mazur, M. M.; Buck, A. C.; Wandtke, M. E.; Liu, J.; Ebraheim, N. A. Prospective Review of Mesenchymal Stem Cells Differentiation into Osteoblasts. *Orthop. Surg.* **2017**, *9*, 13−19.
(47) Wennerberg, A.; Albrektsson, T. Effects of titanium surface topography on bone integration: a systematic review. *Clin. Oral Implants Res.* **2009**, *20* (Suppl 4), 172−184.
(48) Hasegawa, M.; Saruta, J.; Hirota, M.; Taniyama, T.; Sugita, Y.; Kubo, K.; Ishijima, M.; Ikeda, T.; Maeda, H.; Ogawa, T. A Newly Created Meso-, Micro-, and Nano-Scale Rough Titanium Surface Promotes Bone-Implant Integration. *Int. J. Mol. Sci.* **2020**, *21*, No. 783.
(49) Strickstrock, M.; Rothe, H.; Grohmann, S.; Hildebrand, G.; Zylla, I. M.; Liefeith, K. Influence of surface roughness of dental zirconia implants on their mechanical stability, cell behavior and osseointegration. *BioNanoMaterials* **2017**, *18*, No. 20160013, DOI: 10.1515/bnm-2016-0013.

https://doi.org/10.1021/acsomega.4c02322
ACS Omega 2024, 9, 29544−29556